J Mater Sci (2010) 45:2466–2473
DOI 10.1007/s10853-010-4218-9

Effect of particle size in Ni screen printing paste of incompatible polymer binders

J. H. Sung · J. Y. Lee · S. Kim · J. Suh · J. Kim · K. H. Ahn · S. J. Lee

Received: 13 September 2009 / Accepted: 9 January 2010 / Published online: 21 January 2010

Abstract Dispersion of nano-sized particles at high solid content has attracted attention in many industrial applications such as printed electronic products. However, the material design and processing heavily depends on experience with little quantitative measure. For fabrication of thinner dielectric layers, Ni size is getting smaller when used as an inner electrode in multilayer chip capacitor (MLCC). In the present study, we investigate the rheological properties and printing performance of the pastes with two different sizes of Ni particles in the same incompatible binder mixtures of ethyl cellulose (EC) and polyvinyl butyral (PVB). The difference in particle size causes different microstructural heterogeneity and highly nonlinear rheological properties upon the external flow field. The printing pattern and the surface profile are also analyzed by confocal images after screen printing. For smaller particle size of Ni, the more heterogeneous microstructure is observed with increasing PVB content, which is evidenced by the screen printing images as well as its rheological behavior. We explain the difference of spatial heterogeneity in terms of different interactions between particle–particle and particle–polymer. This work is believed to contribute to better design of inner electrodes and processing in MLCC manufacturing.

J. H. Sung · J. Y. Lee · S. Kim · K. H. Ahn (✉) · S. J. Lee
School of Chemical and Biological Engineering, Seoul National University, San 56-1 Shillim-dong, Gwanak-gu, Seoul 151-744, Korea
e-mail: ahnnet@snu.ac.kr

J. Suh · J. Kim
Material Development Group, LCR Division, Samsung Electro-Mechanics Co., Ltd, 314, Youngtong-Gu, Suwon, Gyunggido 443-743, Korea

Introduction

Multilayer ceramic capacitor (MLCC) comprises of alternating layers of inner electrodes and ceramic dielectrics connected in parallel. MLCC requires highly volume efficient and high-capacitance properties despite reduced layer thickness, which can be realized by controlling key factors such as increased number of active dielectric layers, wide overlapped area, precious stacking of the electrodes, and developed high dielectric formulation. Difficulty in manufacturing process lies in the use of submicron- or even nanosized dielectric powders and the application of layer deposition techniques, which originates from the difficulty in layer handling due to severely reduced thickness. Ni is preferred as the internal electrode material due to cost advantage with high capacitance. Fabrication technology for thin-dielectric-layer Ni-MLCC has been progressed under the goal of larger capacitance with thinner dielectric layers, which can be realized with finer dielectric and electrode powders [1]. The Ni electrode continuity and the dielectric-electrode interfacial microstructure strongly affect the electrical properties of the multilayer capacitors. That is, the total capacitance of MLCC depends on the effective area of internal electrodes, and the total resistance depends on the interfacial contact resistance between the Ni electrodes and dielectric layers. The correlation between the heating rate and the thickness of an interfacial layer was reported in terms of electrode continuity [2] and the dependence of the electrical characteristics on the number of dielectric layers were explained in terms of the residual stress [3]. The interfacial layer between the Ni electrodes and $BaTiO_3$ dielectric layer has been studied by accelerating the discontinuity of Ni electrodes during the sintering process.

Ni paste for inner electrode is composed of various organic additives such as dispersant, solvent, and polymer

binders. Paste is a system with high concentration of particles in polymer binder solution, which is required to control the dispersion and the rheological properties. Paste rheology strongly affects the processing condition depending on the factors such as solid contents, particle size and distribution, component composition, mixing process [4–7], and correlates well with screen printability [8]. In general, the binder plays an important role in highly filled particle system for dispersion purpose. When the excess amount of binder is used in the paste system, the final film is formed with lower particle density after sintering caused by the porosity of binder burnout. When the amount of binder is not sufficient to disperse the particles, they tend to aggregate resulting in coarse network structure of the paste, which may cause crack or separation during or after drying process. As the role of a binder is important in paste design, there have been many studies on the kinds of polymer binders like ethyl cellulose (EC) [8, 9] or polyvinyl butyral (PVB) [10, 11], different solvent condition [12], and the effect of dispersant [13]. Polymer binder bridges the particles depending on the affinity of the binder and the particles. However, little has been studied on the effect of a binder on the rheology of the electrolyte paste for the optimization of the screen-printing process as in MLCC manufacturing process.

Most dispersions show non-Newtonian behavior which exhibits both viscous and elastic properties. The viscoelastic behavior of the concentrated particle system includes the time-dependent flow phenomena such as thixotropy and rheopexy, or shear-dependent phenomena like shear thinning or shear thickening which involves the formation or breakdown of the structures. The system depends both on the solid particles and the continuous phase. In particle/polymer mixtures, the dispersion stability is mainly determined by particle–polymer or particle–particle interaction. Adsorbed polymer can lead to steric stabilization in a good solvent or flocculation in a poor solvent. Non-adsorbing polymer can be a repulsive barrier or alleviate attractive depletion effect in a good solvent. The polymer–solvent interaction can be another factor affecting the dispersion state of the suspension. The polymer chains can be further extended in a good solvent since the polymer–solvent attraction is stronger than the polymer–polymer attraction. The conformational degree of freedom may decrease with overlapping of the polymers as the particles come close to each other. This is because the compatibility of a polymer system depends on the interaction between the solvent and the polymer as well as between two different polymers [14]. For better control of the microstructure of the electrodes and higher performance, smaller size of Ni particle is required for thinner electrode and sometimes it is promising to use multibinder system to satisfy the performance, for example, to use EC for good printing and leveling and PVB for excellent adhesion. When the particle size decreases or other component such as secondary binder is added, the dispersion state of the paste can change dramatically, which may lead to many challenging problems in the relevant industry.

The purpose of the present work is to investigate the size effect of Ni paste in incompatible polymer binder system. In this work, the compatibility of EC and PVB at various compositions and its effect was studied using the rheological methodology. The microstructure of the paste and the surface images after screen printing were also investigated, and the rheological properties were correlated with the dispersion state of the paste.

Experiments

Preparation of Ni paste

Ni powder used in this study (Shoei Chemicals Company, Japan) has BET-specific surface area of 6 ± 0.5 m^2/g, density 5.8×10^3 kg/m^3, and the mean particle diameter of 120 and 180 nm. Dihydroterpineol acetate (DHTA, Nippon Terpene Chemicals Inc., Japan) was used as a suspending medium. DHTA-based Ni paste system containing long chain fatty acid alkyl amine salt (ED116, Kusumoto Chemicals Ltd., Japan) as a dispersant was used with two different polymer binders. For good printability and leveling performance of Ni paste, ethyl cellulose (EC, Dow Chemical Corp.) having an ethoxyl content of 48.0–49.5 wt% and the molecular weight of 1.91×10^5 g/mol was used. Poly(vinyl butyral) (PVB, Sekisui Chemical, Japan) with the molecular weight of 3.6×10^5 g/mol, which shows excellent adhesion with green sheet was also used as a binder. Ni pastes were composed of 8.3 ± 0.0 vol.% solid particles dispersed in organic solvent with 2.7 ± 0.2 wt% polymer binders and 0.8 ± 0.1 wt% dispersant based on the weight of the Ni powder. We prepared five samples with different compositions of two binders for each Ni particle size (120 and 180 nm), respectively. The ratio of EC:PVB in Ni paste was changed as 100:0, 70:30, 50:50, 30:70, and 0:100, keeping the total amount of polymer binders as 2.7 ± 0.2 wt% based on the weight of Ni powder. We named the paste systems as EC10PVB0, EC7PVB3, EC5PVB5, EC3PVB7, and EC0PVB10 based on the binder composition. Ni paste was dispersed and stored using a 3-roll mill for phase stability.

Rheological properties of Ni paste

Rheological properties were characterized using a controlled strain rheometer (ARES, TA Instruments) with a parallel plate fixture and gap size of 1 mm. Each sample

was loaded and relaxed for 30 min prior to measurement. Cone and plate geometry was used to measure the viscosity of dilute polymer solutions, whose diameter was 50 mm and cone angle was 0.04 rad.

Screen printing

Screen printing was performed at 300 mm/s of printing speed with C400 mesh, 2.0 mm of snap-off distance, and 7.5 kgf/cm^2 of squeegee pressure.

Surface characterization of dried film

Printed surface was observed by using a confocal laser scanning microscope (CLSM, OLS3000, LEXT) with a semiconductor laser ($\lambda = 408 \pm 5$ nm) after drying. A scanning type laser microscope scans over the specimen in x–y direction. In addition, the surface in z-direction can be recognized by repelling light that comes from place other than focusing position. One-dimensional surface profiler (Alpha-step) which has a resolution of 0.1 nm in z-direction and 0.01 μm in x-direction was used.

Results and discussion

Ni paste used for inner electrode in MLCC manufacturing requires the performance of the final film which should be as dense as possible, no defect, and moderate shrinkage of the substrate during drying and sintering. Among the components in the paste with highly filled particle contents, the most important one is the binder which plays a key role in optimizing the film microstructure. The paste shows complicated rheological behavior depending on deformation history, which is strongly correlated with screen printing process and affects the morphological characteristics after drying process.

Figure 1 shows the shear viscosity (a) and dynamic moduli (b) as a function of composition ratio of two binder polymers. Shear thinning behavior is observed due not only to the alignment of the particles but also to the orientation of the polymer chains with increasing shear rate. EC10PVB0 shows the highest viscosity and EC0PVB10 shows the lowest value. The frequency dependence shows that the loss modulus (G'') is larger than the storage modulus (G') irrespective of the composition, and EC10PVB0 is more elastic than EC0PVB10. When the particles are dispersed in polymer matrix, the high frequency behavior originates from the characteristics of the polymer matrix, and the low frequency behavior reflects the microstructural details of the particle dispersion in particular. The low frequency moduli increase with EC

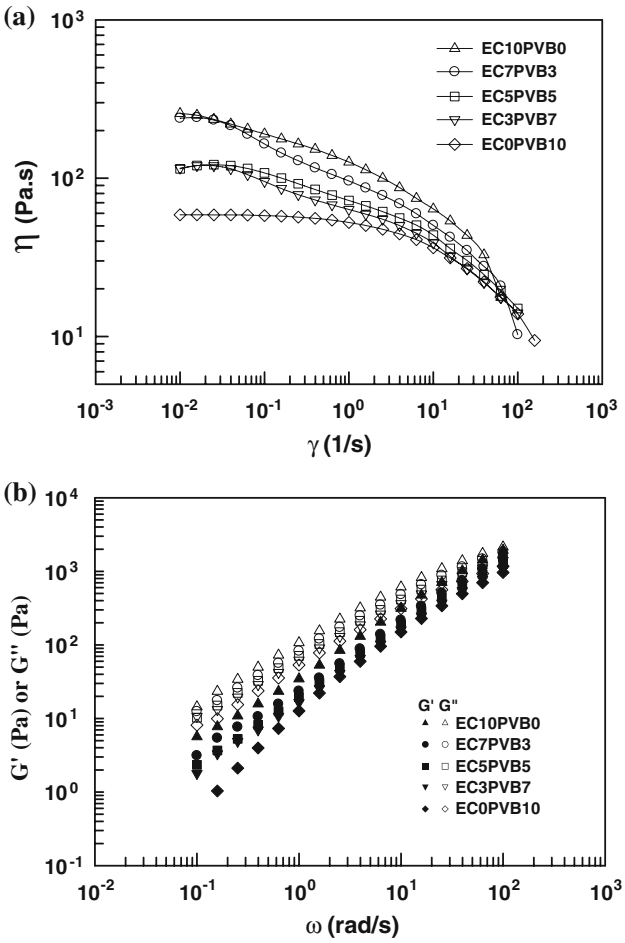

Fig. 1 **a** Shear viscosity and **b** dynamic moduli of 180 nm Ni pastes at different binder compositions

content, which implies that EC forms stronger percolating network of flocs compared to PVB.

Figure 2 shows the viscosity of Ni paste with different particle size (a) 180 nm and (b) 120 nm dispersed in different binder solutions. Shear viscosity is higher in 120 nm Ni paste system than that of 180 nm Ni paste by an order of magnitude and rapidly decreases with shear rate. Shear thinning has been attributed to the alignment of the particles into layers which may slip or distorts the existing structural order. The highly filled paste forms a structured network that is gradually broken when the shear is applied. The paste with 120 nm Ni forms stronger network structure at low shear rate compared to the paste with 180 nm Ni, which is evidenced by the larger viscosity. Although it is a well-dispersed system, the flocs or aggregates are unavoidable, leading to size distribution and local heterogeneity. The effect of size distribution on viscosity depends on particle–particle interaction and the softness of the particle surface [15]. Due to this local heterogeneity, the structure of the paste adjacent to a solid boundary can be different from that in the bulk. As a consequence, the rheological

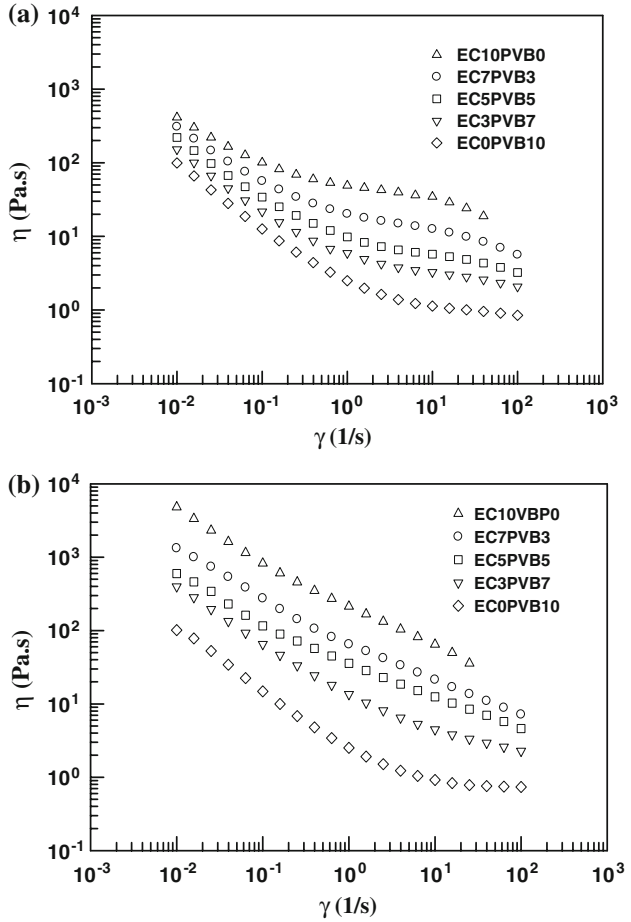

Fig. 2 Shear viscosity of Ni paste with different size **a** 180 nm and **b** 120 nm

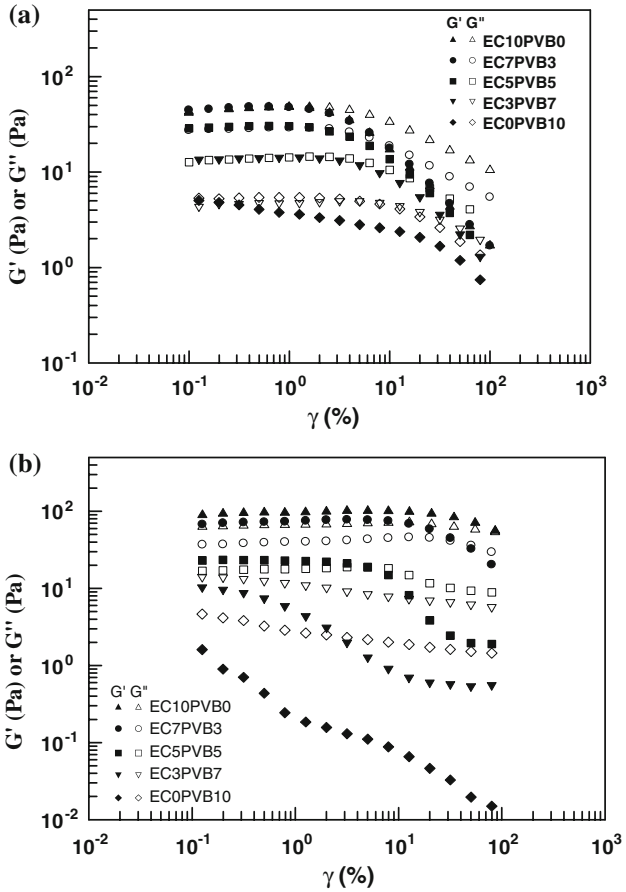

Fig. 3 Strain amplitude sweep test of Ni pastes with two different particle sizes **a** 180 nm and **b** 120 nm at different ratio of two binders

properties at the boundary differ from those of the bulk and induce a wall effect [16].

The viscoelastic properties of the paste are determined by the balance of the interactions and forces; Brownian force, hydrodynamic interaction, and interparticle forces (i.e., van der Waals attraction, steric interaction, double layer repulsion, etc.). They are governed by many factors such as volume fraction, particle size, shape distribution, surface chemistry, and ingredients. The rheology of the concentrated suspension is complex and heavily depends on deformation history. Figure 3 shows the strain sweep test results with two different size (a) 180 nm and (b) 120 nm Ni pastes at a frequency of 0.1 rad/s. The curves remain constant at small strain, and then start to decrease at certain strain amplitude, so called the 'critical strain' (γ_{crit}). All the pastes that include EC binder in 180 nm Ni paste system show the linear viscoelastic region where the microstructure is unperturbed from the external flow field and the strain-independent behavior is observed (constant modulus). At high strain, G' decreases due to the breakdown of internal microstructure resulting in the nonlinear viscoelastic behavior. Interesting is the reverse trend of G' in 180 and 120 nm Ni pastes with strain. The critical strain in Fig. 3a slightly increases as PVB content increases, except for EC0PVB10. However, the critical strain in Fig. 3b significantly decreases as PVB content increases. We have no clear understanding yet for this reversal, but it clearly shows the difference from different particle size. In addition, the cross-over point ($G' = G''$) gradually shifts to higher strain in 180 nm Ni paste system as PVB content increases. However, in 120 nm Ni paste, the cross-over point shifts to lower strain; for example, at $\gamma = 50$ for EC7PVB3 and at $\gamma = 5$ for EC5PVB5. When the strain increases further, a breakup of network occurs and the paste experiences a transition into the liquid-like state. This phenomenon leads to shorter linear viscoelastic region with increasing PVB content in 120 nm Ni paste. Correlation between the microstructure and the rheological properties with different Ni size dispersed in binary binder solution will be discussed later.

Figure 4 shows the surface images of screen printed film from (a) 180 nm and (b) 120 nm Ni pastes with different ratio of EC and PVB binders. Printing quality is better for

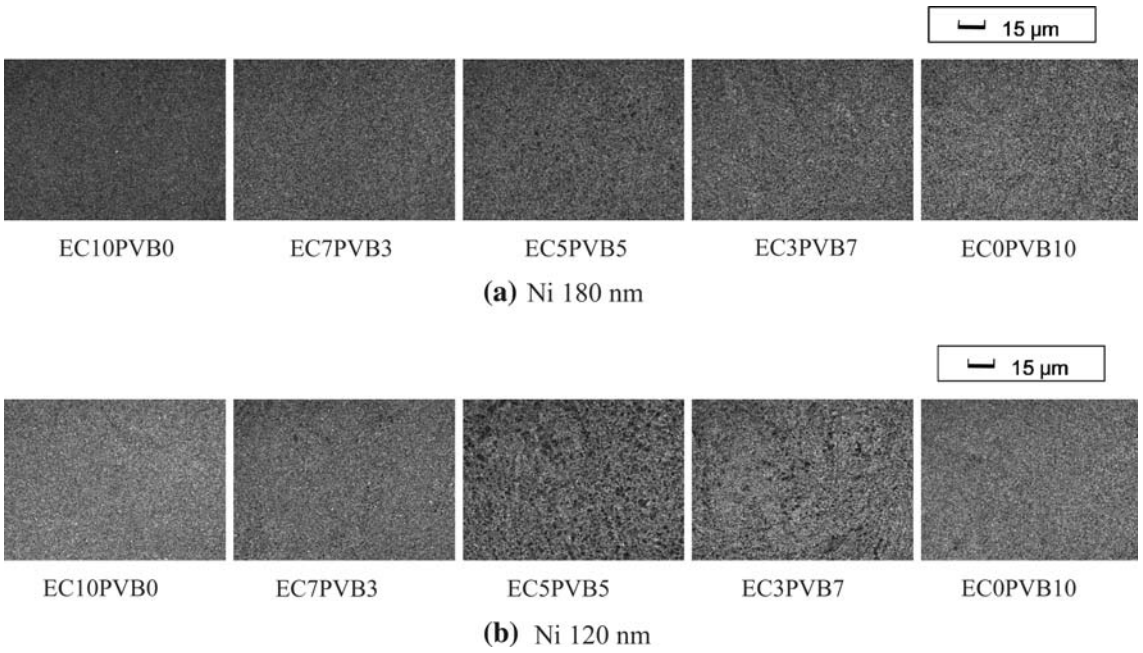

Fig. 4 Confocal images of printing surface of Ni pastes with different particle size **a** 180 nm and **b** 120 nm at various ratio of binder mixtures

180 nm Ni paste than 120 nm Ni paste, more pronouncing in multibinder systems. The fact that the linear viscoelastic region becomes narrower as PVB content increases implies less stable microstructure which is hard to withstand the deformation. It can be related to poor surface profile especially in EC5PVB5 and EC3PVB7. The printing surface roughness measured from the profile images in which the intensity of the picture at each point has a linear relation with the height of the surface is given in Fig. 5. The pastes with 180 nm Ni powder show good printing surface as evidenced by a small mean deviation of the height. However, it becomes worse as the particle size decreases especially at the binder ratio of 50:50 and 30:70. The microstructure of the film depends on many parameters such as particle size, kind, and amount of binder, leading to diverse microstructures such as pore and crack when excess and insufficient binder is used, respectively.

In the present work, two polymer binders were used to obtain synergic effect for both good printability and good adhesion to the printed multilayers. Understanding the compatibility between the polymer and solvent is important for better design of the paste. By calculating the Huggins constant (K_H) [17], the affinity of the polymer and solvent can be estimated. It was calculated as 0.28 for EC/DHTA and 0.62 for PVB/DHTA, respectively. A useful criterion is; 0.52 in theta solvent, smaller than 0.52 in good solvent, and larger than 0.52 in poor solvent [14]. Therefore, DHTA is believed to be a good solvent for EC and poor solvent for PVB, so that EC may lead to stabilization and PVB to flocculation. We expect that the dispersion stability is governed by PVB. Poor dispersion caused by PVB may lead to phase separation and to poor surface quality after coating and drying. The Huggins equation could be expanded to the ternary system which is composed of polymer A/polymer B/solvent as follows:

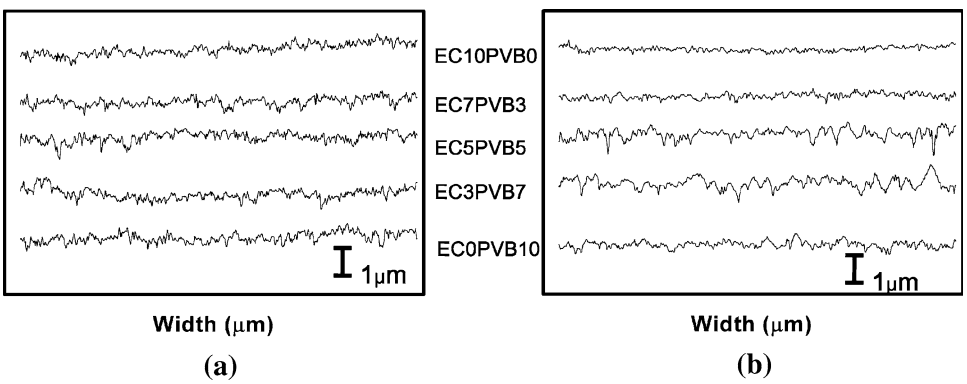

Fig. 5 Profile images of printing surface roughness of **a** 180 nm and **b** 120 nm Ni pastes

$$\frac{(\eta_{sp})_m}{c_m} = [\eta]_m + b_m c_m = [\eta]_m + k_m [\eta]^2 c_m \quad (1)$$

where $c_m = c_A + c_B$ is the total polymer concentration, and $[\eta]_m$, b_m, k_m are the intrinsic viscosity, the Huggins slope coefficient, and the Huggins constant of two polymer mixtures (subscript m), respectably. We used the "ideal" value of the viscometric interaction parameter from $b_{AB}^{id} = (b_A b_B)^{0.5}$ and the experimental value of b_{AB} which can be determined from the interaction term b_m in the Huggins equation for a ternary polymer solution.

$$b_m = b_A \omega_A^2 + b_B \omega_B^2 + 2 b_{AB} \omega_A \omega_B \quad (2)$$

The compatibility can be accounted for by the difference between the experimental and ideal values, in a given solvent and mixture composition.

$$\Delta b_{AB} = b_{AB} - b_{AB}^{id} \quad (3)$$

This provides a criterion of compatibility, which can be classified as follows;

if $\Delta b_{AB} > 0 \quad (b_{AB} > b_{AB}^{id})$: compatible or attractive interaction
if $\Delta b_{AB} < 0 \quad (b_{AB} < b_{AB}^{id})$: incompatible or repulsive interaction
if $\Delta b_{AB} = 0 \quad (b_{AB} = b_{AB}^{id})$: chains do not interact favorably nor unfavorably

Figure 6 shows Δb_{AB} as a function of weight fraction of PVB in the EC/PVB/DHTA solution. At $\omega_{PVB} = 0.3$, two polymers could be compatible, while incompatible at $\omega_{PVB} = 0.5$ and 0.7. The Huggins constant k_{AB} which expresses the degree of interaction between two polymers can be derived using $k_{AB}^{id} = (k_A k_B)^{0.5}$ *and* $\Delta k_{AB} = k_{AB} - k_{AB}^{id}$ from the following equations.

$$b_{AB} = k_{AB} [\eta]_A [\eta]_B \quad (4)$$

$$k_{AB} = \frac{b_m - (b_A \omega_A^2 + b_B \omega_B^2)}{2[\eta]_A [\eta]_B \omega_A \omega_B} \quad (5)$$

Polymer blend is compatible if $\Delta k_{AB} > 0$ and incompatible if $\Delta k_{AB} < 0$. The expansion of the classical Huggins equation was applied to calculate the EC/PVB interaction parameters in the solution state. Here again it is clear that two polymers are compatible at $\omega_{PVB} = 0.3$ while incompatible at $\omega_{PVB} = 0.5$ and 0.7.

In MLCC manufacturing as in other industry, it is important to understand the fundamental relationship of rheology, morphology, and processing for better design of material and processing. The rheological behavior and morphology is closely correlated. For example, the dispersion state of the paste is reflected on its rheological properties. We now analyze in depth how the size of Ni affect the rheology of the Ni paste dispersed in the same incompatible two binder mixtures. In Fig. 3, we showed an interesting rheological behavior as a function of strain as the binder composition changes. The critical strain (γ_{crit}) behaved in different way for different particle size, which implies that the microstructure is quite different for pastes of different particle size. EC0PVB10 did not show the linear viscoelastic region within the range of our measurement regardless of the particle size. Figure 7 plots γ_{crit} of the pastes with different composition of two binder mixtures based on G' and G''. γ_{crit} slightly increases in 180 nm Ni paste (this is more clear when the critical strain is based on G''), while significantly decreases in 120 nm Ni paste with increasing PVB content. For comparison, γ_{crit} of the binder mixtures with no Ni particles is about 50% for all blends except homo PVB binder system. As the strain increases beyond the critical strain, a breakup of network occurs and the material experiences a transition into the liquid-like state, which is more pronounced in 120 nm Ni paste system.

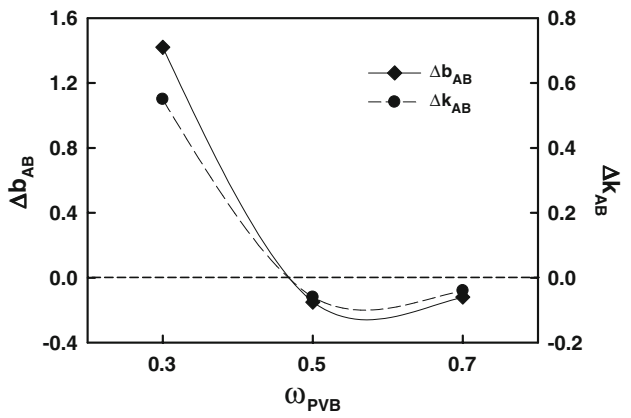

Fig. 6 Thermodynamic interaction parameter Δb_{AB} and Δk_{AB} vs. ω_{PVB} in EC/PVB/DHTA solutions

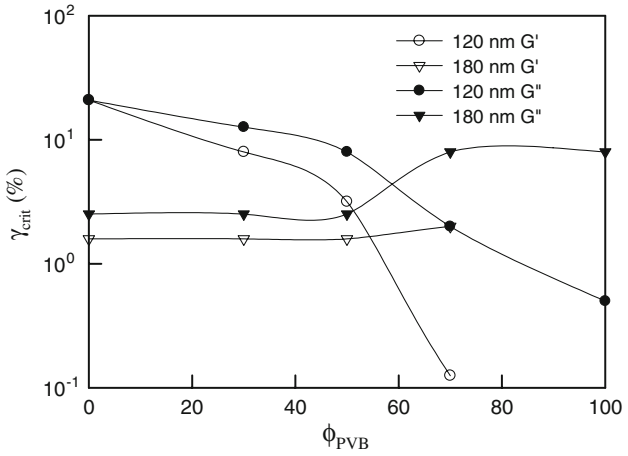

Fig. 7 Critical strain of 180 and 120 nm Ni pastes with different PVB compositions

The only difference in this study is the particle size, which implies that the microstructure is different with different particle–particle and particle–polymer interaction. Thus, the microstructure of the paste which is locally heterogeneous responds to the external flow field in different ways. Phase stability can be accounted for in terms of the molecular contacts between particle and medium [18]. This result suggests a possible polymer bridging which is governed by the strength of the spatial steric interactions. In dense system, the adsorbed conformation strongly depends on the affinity to the particle surface, which is often controlled by the addition of a dispersant or a surfactant [19]. From the above viscometric approach, it can be concluded that PVB can lead to unstable microstructure which is hard to withstand the deformation under the flow field, especially in 120 nm Ni paste system.

Figure 8 shows G' of 120 and 180 nm pastes in linear and nonlinear viscoelastic region, before and after γ_{crit}. The strain for linear region was selected as 0.05% for 120 and 180 nm pastes, and the strain for nonlinear region was selected as 12 and 10% for 120 and 180 nm pastes, respectively. The microstructure of 120 nm Ni paste at small strain does not change much, while it shows a rapid breakdown with increasing PVB component at large deformation in nonlinear regime. On the other hand, G' of 180 nm Ni paste does not change much regardless of the strain, whether it is in linear or in nonlinear region. Smaller particles possibly lead to the enhanced heterogeneous microstructure such as local phase separation developed by external flow field. It can be induced by the migration of the particles toward preferred phase of two components [20–22], or by the interaction between particles of the same size in polydisperse particle system [23]. Even though the same incompatible binder mixture was used, the rheological behavior was significantly different. The difference in rheology which is formed from different particle size is caused by the locally different density profile and different interactions in the microstructure.

The viscosity of the dispersion depends on the volume occupied by the particles, and numerous equations have been proposed to relate viscosity to the volume fraction of the particles. For example, Einstein's equation shows the intrinsic viscosity as a function of volume fraction in dilute dispersion which is independent of the particle size or size distribution. However, in practical applications, the flow and consequently the viscosity are affected by spatial distribution between the particles and by the particle–particle interactions resulting in complex microstructure formation. Figure 9 shows the reduced shear viscosity $(\eta_{paste}/\eta_{medium})$ as a function of shear rate for different ratio of two polymer mixtures. Shear thinning behavior is common as in Fig. 2, however, the reduced viscosity exhibits slight shear thickening behavior at higher shear rate. Shear thickening behavior in 180 and 120 nm Ni paste becomes more

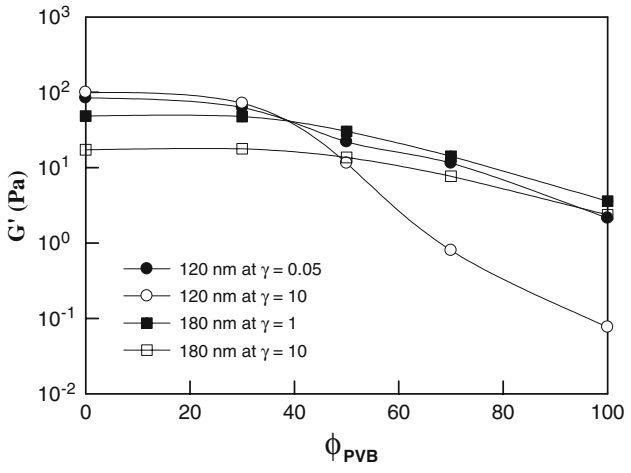

Fig. 8 Storage modulus at strain 0.05% as a linear region of both pastes, and at 12 and 10% as a nonlinear region of 180 and 120 nm Ni pastes, respectively, with different PVB compositions

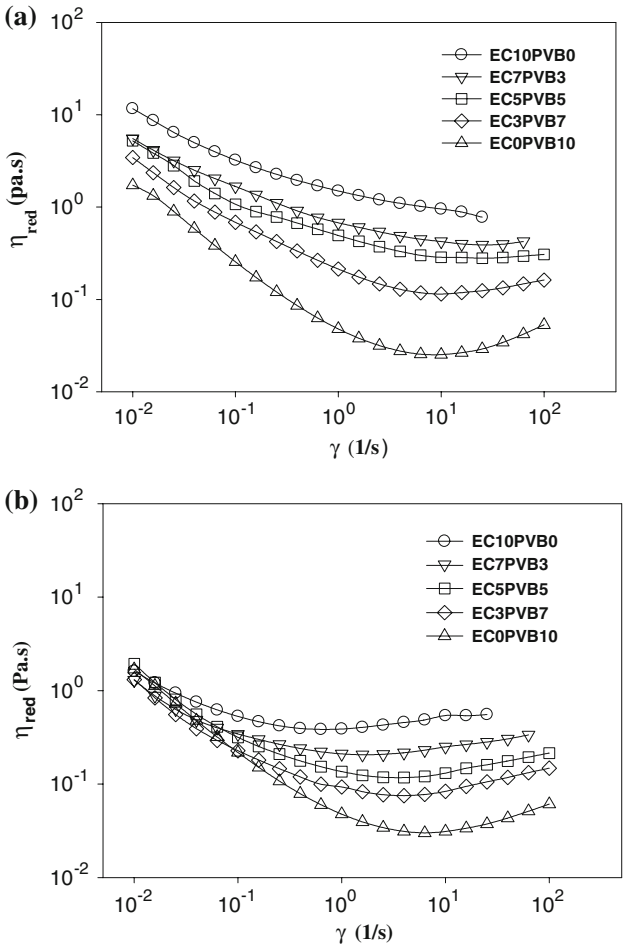

Fig. 9 Reduced shear viscosity of Ni pastes with two different particle sizes **a** 180 nm and **b** 120 nm at different ratio of two binders

pronounced with increasing PVB content in two binder mixtures and homo PVB medium. In polymer solutions, shear thickening may be induced by the decrease in entropy of polymer chains forming the network structure during deformation by shear. In suspensions, the extension of the polymer coils bridging the particles may provide additional energy dissipation. Shear thickening seems to be induced by the enhanced resistance due to the chain extension of the polymer bridges, but it is yet clear why it becomes more pronounced with increasing PVB content.

Conclusion

We investigated the microstructural heterogeneity of Ni pastes with different size of Ni particles dispersed in incompatible binder mixtures. The rheological behavior of the pastes was rich, and provided useful information on the microstructure, which was determined not only from the dispersed state of the particles but also from the local interface change induced by the flow field. Rheology of Ni paste shows quite different behavior when different size of the particles was used, while the other factors remaining the same. The nonlinear behavior showed a reverse trend for 180 and 120 nm Ni pastes, respectively. γ_{crit} slightly increased in 180 nm Ni paste, while it significantly decreased in 120 nm Ni paste with increasing PVB content. The microstructure of the Ni paste became more heterogeneous in less stable medium upon the external flow field. The smaller particle size of Ni showed more heterogeneous microstructure with increasing PVB content, which was evidenced by the screen printing profiles. Shear thickening in the reduced viscosity was also observed at high shear rate, which seems to be induced by the enhanced resistance due to the chain extension of the polymer bridges.

Acknowledgement This study was supported by the Korea Research Foundation (KRF) Grant funded by the Korea government (MEST) (2009-0070200).

References

1. Kishi H, Mizuno Y, Chazono H (2003) Jpn J Appl Phys 42:1
2. Polotai AV, Fujii I, Shay DP, Yang GY, Dickey EC, Randall CA (2008) J Am Ceram Soc 91:2540
3. Nakano Y, Nomura T, Takenaka T (2003) Jpn J Appl Phys 42:6041
4. Tseng WJ, Chen CN (2006) J Mater Sci 41:1213. doi: 10.1007/s10853-005-3659-z
5. Scirocco R, Vermant J, Mewis J (2005) J Rheol 49:551
6. Nguty TA, Ekere NN (2000) Rheol Acta 39:609
7. Lu K, Kessler C (2006) J Mater Sci 41:5613. doi:10.1007/s10853-006-0303-5
8. Phair JW (2008) J Am Ceram Soc 91:2130
9. Lee S, Paik U, Yoon SM, Choi JY (2006) J Am Ceram Soc 89:3050
10. Lewis JA, Blackman KA, Ogden AL, Payne JA, Francis LF (1996) J Am Ceram Soc 79:3225
11. Blackman K, Slilaty RM, Lewis JA (2001) J Am Ceram Soc 84:2501
12. Renger C, Kuschel P, Kristoffersson A, Clauss B, Oppermann W, Sigmund W (2007) J Eur Ceram Soc 27:2361
13. Thwala JM, Goodwin JW, Mills PD (2008) Langmuir 24:12858
14. Hong PD, Huang HT, Chou CM (2000) Polym Int 49:407
15. D 'Haene P, Mewis J (1994) Rheol Acta 33:165
16. Hutton JF (1975) Rheol Acta 14:979
17. Huggins ML (1942) J Am Chem Soc 64:2716
18. Mackay ME, Tuteja A, Duxbury PM, Hawker CJ, von Horn B, Guan Z, Chen G, Krishnan RS (2006) Science 311:1740
19. Horigome M, Otsubo Y (2002) Langmuir 18:1968
20. Wu G, Asai S, Sumita M, Yui H (2002) Macromolecules 35:945
21. Ginzburg VV (2005) Macromolecules 38:2362
22. Laradji M (2004) J Chem Phys 120:9330
23. D'Aguanno B, Wagner NJ (1990) Mat Res Soc Symp Proc 177:219